

Kagome superconductors from Pomeranchuk fluctuations in charge density wave metals

Yu-Ping Lin¹ and Rahul M. Nandkishore^{1,2}

¹*Department of Physics, University of Colorado, Boulder, Colorado 80309, USA*

²*Center for Theory of Quantum Matter, University of Colorado, Boulder, Colorado 80309, USA*

(Dated: July 20, 2021)

Motivated by the recent experiments on the kagome metals AV_3Sb_5 with $A = K, Rb, Cs$, which see onset of charge density wave (CDW) order at ~ 100 K and superconductivity at ~ 1 K, we explore the onset of superconductivity, taking the perspective that it descends from a parent CDW state. In particular, we propose that the pairing comes from the Pomeranchuk fluctuations of the reconstructed Fermi surface in the CDW phase. This scenario naturally explains the large separation of energy scale from the parent CDW. Remarkably, the phase diagram hosts the double-dome superconductivity near two reconstructed Van Hove singularities. These singularities occur at the Lifshitz transition and the quantum critical point of the parent CDW. The first dome is occupied by the d_{xy} -wave nematic spin-singlet superconductivity. Meanwhile, the $(s + d_{x^2-y^2})$ -wave nematic spin-singlet superconductivity develops in the second dome. Our work sheds light on an unconventional pairing mechanism with strong evidences in the kagome metals AV_3Sb_5 .

The recently uncovered kagome metals AV_3Sb_5 with $A = K, Rb, Cs$ have drawn enormous attention due to a host of unconventional correlated phases. The charge density waves (CDW) have been observed at high critical temperature ~ 100 K [1–26]. These orders develop at three commensurate momenta, and are believed to be driven by the nesting of the Fermi surface, further enhanced by the M -point Van Hove singularity. The bond density modulations of these $3Q$ orders form the star-of-David or inverse star-of-David patterns [27–35]. The giant anomalous Hall effects indicate nontrivial band topology under time-reversal symmetry breaking [2, 6], which may be attributed to the onset of loop currents [5, 16, 19, 24, 28–31, 33, 36–41]. Meanwhile, the possibility of higher-order topological insulators have also been proposed [42]. The breakdown of C_6 symmetry is observed generally in the experiments. This symmetry breaking may be related to the unequal complex phases of $3Q$ orders [42] or the intertwinement between three-dimensional orders [31, 34, 35]. At lower temperature, a $1Q$ modulation with halved momentum also adds a new color to the rich correlated phenomena [8, 11, 16, 19].

More exotic phenomena have been observed from the superconductivity (SC) [3, 6, 7, 9, 11, 21, 22, 26, 43–52]. The onset of superconductivity occurs at a much lower critical temperature ~ 1 K, where the breakdown of C_6 symmetry persists [49, 50]. Remarkably, the superconductivity exhibits a double-dome structure under pressure, which extends above the critical pressure of the CDW [7, 22, 46]. New superconducting domes can even appear at much higher pressure [7, 48, 52]. Despite the experimental observations of rich phenomena, a thorough theoretical understanding remains elusive. Given the proximity to Van Hove singularity, the superconductivity may be treated as a competing instability with the CDW [53]. This competing-order scenario may explain the opposite trends of these states, where the critical tem-

peratures evolve oppositely under pressure [7, 22, 48, 52] and uniaxial strain [26]. However, the scenario does not fit the large separation of energy scales at ambient pressure. This suggests an alternative scenario, which should explain the large separation of energy scales as well as the exotic double-dome superconductivity under pressure.

In this Letter we propose an alternative mechanism that appears consistent with the salient experimental

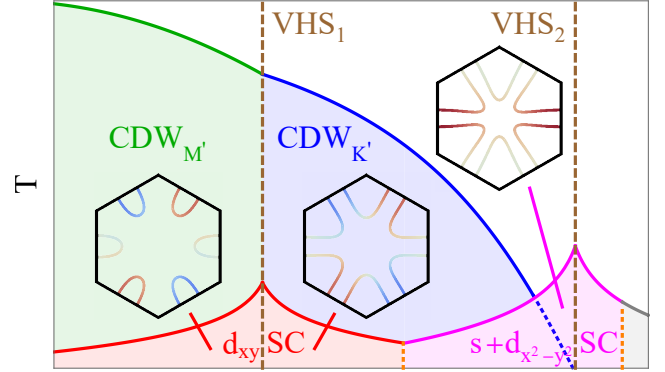


FIG. 1. Schematic illustration of the phase diagram in our theoretical model. The vertical axis denotes the temperature T , while the horizontal axis takes any parameter whose variation drives the CDW to a quantum critical point. The insets indicate the reconstructed Fermi surfaces in the reduced Brillouin zone, where two Van Hove singularities ($VHS_{1,2}$) can occur. The first one separates the CDW with the Fermi pockets at M'_α and K'_α ($CDW_{M',K'}$), while the second one marks the recovery of noninteracting Fermi surface at the quantum critical point. At low temperature, the reconstructed Pomeranchuk fluctuations induce the double-dome superconductivity. The critical temperature peaks at the two reconstructed Van Hove singularities. Different leading channels are manifest in the two domes, where the gap functions are shown on the reconstructed Fermi surfaces. The regime far above the quantum critical point is beyond our theoretical model.

facts. We adopt the perspective that the CDW is a ‘parent’ phase, and that the superconductivity emerges from the fluctuations thereof - naturally explaining the large separation of energy scales. Specifically, we propose the pairing comes from the Pomeranchuk fluctuations of reconstructed Fermi surface in the CDW phase. Remarkably, this mechanism not only naturally explains the separation of energy scales, but it also predicts a double-dome structure for the superconductivity under pressure (Fig. 1) [7, 22, 46], with the critical temperature peaking near two reconstructed Van Hove singularities.

We start by introducing the reconstructed band structures of Van Hove CDW on the kagome lattice. The Van Hove Fermi surface is a hexagon in the hexagonal Brillouin zone. The corner saddle points sit at the zone edge centers $\mathbf{M}_{\alpha=1,2,3}$ [Figs. 2(a) and 2(b)], where the density of states experiences the logarithmic Van Hove singularity [54]. Various Fermi liquid instabilities are enhanced at this singularity [31, 41, 55–61]. With the nesting between opposite Fermi lines, CDW can develop at three nesting momenta $\mathbf{Q}_{\alpha} \equiv \mathbf{M}_{\alpha}$. Due to the doubled periodicity under commensurate momenta $2\mathbf{Q}_{\alpha} \equiv 0$, the bands are folded quadruply onto the $1/2 \times 1/2$ reduced Brillouin zone. The noninteracting Fermi surface is folded into three lines between the zone edge centers $\pm\mathbf{M}'_{\alpha}$, where a crossing occurs at the zone center Γ . The energetically favored ground states are the $3Q$ orders with simultaneous ordering at all momenta [30]. These $3Q$ orders maximize the gap structures by gapping the Fermi surface, leaving three low-energy valleys at \mathbf{M}'_{α} in the reconstructed band structures [30, 40]. A low-energy patch model is defined by the three-component fermion $\psi = (\psi_1, \psi_2, \psi_3)^T$ from these valleys (Fig. 3). The CDW manifests itself in the valley gaps at low energy, which turn into the characteristic deformation energy $\tilde{\Delta} = \Delta\hat{n}$ with $\Delta > 0$ and $\hat{n} = \hat{n}_{111} = (1/\sqrt{3})(1, 1, 1)$ in the patch model.

Importantly, the Van Hove Fermi surface may not exhibit an ideal hexagon in practical systems [Figs. 2(a) and 2(b)]. With further neighbor hoppings, distorted Fermi lines with nonperfect nesting can lead to the residual Fermi pockets at \mathbf{M}'_{α} [Fig. 2(c)]. These Fermi pockets may be enlarged by, for example, deformations of the noninteracting Fermi surface at finite doping. The suppression of the CDW at finite doping further amplifies the enlargement of the Fermi pockets. Significantly, a Lifshitz transition may occur and manifest a reconstructed Van Hove singularity. This Lifshitz transition is driven by the maximization of gap structures, where the enlarged Fermi pockets at \mathbf{M}'_{α} lose the energetic favor to those at the zone corners \mathbf{K}'_{α} [Fig. 2(d)]. The presence of such a transition may be observed, for example, from a CDW transition in a Ginzburg-Landau analysis [31]. Whether the transition occurs in the CDW phase is system-dependent. When the CDW vanish at a critical doping, the reconstructed Fermi surface recovers its noninteracting form. This marks the occurrence of an-

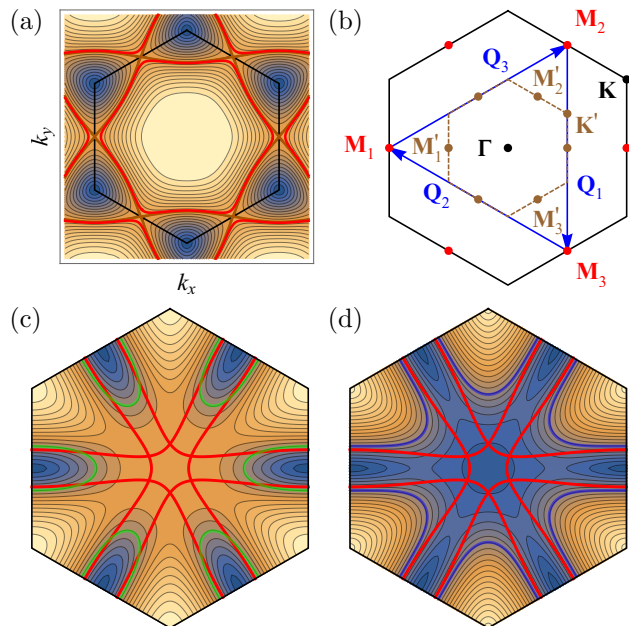


FIG. 2. (a) The highest conduction band on the kagome lattice with nonperfect nesting. The Fermi surfaces (brown) at and (red) away from the Van Hove singularity are illustrated in the (black) hexagonal Brillouin zone. (b) High symmetry points and nesting momenta in the (black) original and (Brown) reduced Brillouin zones. (c)/(d) In the parent CDW, the (red) folded noninteracting Fermi surface is gapped into the (green/blue) Fermi pockets at $\mathbf{M}'_{\alpha}/\mathbf{K}'_{\alpha}$ on the highest reconstructed conduction bands in the reduced Brillouin zone.

other reconstructed Van Hove singularity. Note that the reconstructed Fermi surface can also evolve under the other variations, such as increasing pressure. Any variation that drives the CDW to a quantum critical point can serve as the tunable parameter in our analysis. In the patch model, we allow the patches at \mathbf{k}_P to move along the $\mathbf{M}'_{\alpha}-\Gamma$ lines under the evolution. These patches capture the portions of the Fermi pockets with the largest density of states.

We aim at analyzing how the CDW fluctuations affect low-energy phenomena. A notable consequence is the induction of fluctuations in the reconstructed band structures. In the patch model, the CDW fluctuations are reflected by the fluctuations of the deformation energy. Such fluctuations are clearly depicted in a Bloch sphere model [Fig. 4(a)], where the deformation energy is mapped onto \hat{n}_{111} in the first octant of a Bloch sphere. Three symmetry channels are available to the fluctuations, which contain the modes in one radial and two tangential directions. Significantly, these fluctuations manifest themselves in the Pomeranchuk (POM) channels. These channels manifest the deformations of the reconstructed Fermi surface, whose fluctuations are described by an effective Pomeranchuk coupling

$$H_{\text{POM}}^a = J^a P_{\text{POM},a}^\dagger P_{\text{POM},a}. \quad (1)$$

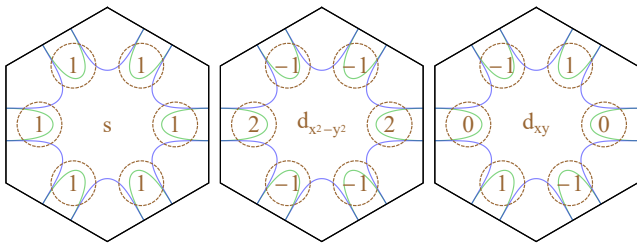


FIG. 3. The patch model in the reduced Brillouin zone. For the Fermi pockets at (green) \mathbf{M}'_α and (blue) \mathbf{K}'_α , the (brown dashed circles) patches are placed at \mathbf{k}_P on the \mathbf{M}'_α - Γ lines. The patch representations are indicated in the irreducible pairing channels.

The Pomeranchuk pairing operators are defined

$$P_{\text{POM},a} = \psi^\dagger \left(\frac{\sigma^0}{\sqrt{2}} \right) d_a \psi \quad (2)$$

with an implicit momentum difference between particle $\psi^\dagger_{\mathbf{k}+\mathbf{q}}$ and hole $\psi_{\mathbf{k}}$ fermions. Here the Pauli matrices $\sigma^0 = 1$ and $\boldsymbol{\sigma} = (\sigma^1, \sigma^2, \sigma^3)^T$ are set in the spin sector. Under C_6 symmetry, there are three irreducible pairing channels for the Pomeranchuk fluctuations (Fig. 3), which map onto the symmetry channels of the deformation energy fluctuations. The s -wave channel with the isotropic patch representation $d_0 = (1/\sqrt{3})\text{diag}(1, 1, 1)$ corresponds to the radial channel. Meanwhile, the $d_{x^2-y^2,xy}$ -wave channels with anisotropic $d_1 = (1/\sqrt{6})\text{diag}(2, -1, -1)$ and $d_2 = (1/\sqrt{2})\text{diag}(0, 1, -1)$ are related to the longitudinal and latitudinal channels, respectively. We assume that the fluctuations are on the verge of instability in certain channels. This is captured by the attractive couplings $J_{\mathbf{q}}^a \sim -J_0^a(q^2 + \xi_a^2)^{-1} < 0$, which are large but nondivergent near the zero momentum $q = 0$ at finite correlation lengths ξ_a . The leading fluctuation occurs in the channel with the largest coupling J_0^a .

Strong Pomeranchuk fluctuations may drive certain Cooper channels attractive and trigger superconductivity [62–64]. To search for attractions, we project the effective Pomeranchuk coupling (1) on the Cooper channels and determine the leading ones [65]

$$H_{\text{SC}}^a = V_s^a (P_{\text{SC},a}^0)^\dagger P_{\text{SC},a}^0 + V_t^a \mathbf{P}_{\text{SC},a}^\dagger \cdot \mathbf{P}_{\text{SC},a}. \quad (3)$$

The singlet and triplet Cooper pairing operators are

$$(P_{\text{SC},a}^\nu)^\dagger = \psi^\dagger \left(\frac{\sigma^\nu}{\sqrt{2}} \right) \tilde{d}_a [(i\sigma^2)(\psi^\dagger)^T]. \quad (4)$$

Here the patch representations $\tilde{d}_{0,2} = d_{0,2}$ inherit the Pomeranchuk ones in the s - and d_{xy} -wave channels, while a $(s + d_{x^2-y^2})$ -wave patch representation $\tilde{d}_1 \approx (1, 0, 0)$ is obtained from the $d_{x^2-y^2}$ -wave Pomeranchuk fluctuation. The according couplings $V_{s,t}^a$ are symmetrized and anti-symmetrized

$$V_{s,t}^a = \frac{1}{2}(J_0^a \pm J_{2\mathbf{k}_P}^a). \quad (5)$$

The symmetrized couplings are stronger according to the form of $J_{\mathbf{q}}^a$. This implies the energetic favor of singlet pairings under strong Pomeranchuk fluctuations. Among the irreducible pairing channels, the leading channel inherits the largest coupling $V_s^a \approx J_0^a/4$ from the leading Pomeranchuk fluctuation. The onset of superconductivity occurs at a critical temperature

$$T_c \approx \Lambda e^{-1/(V_s D)}. \quad (6)$$

Here Λ is an ultraviolet cutoff of the patch model and D is the density of states at the Fermi level.

We now construct the phase diagram (Fig. 1) of the superconductivity and the parent CDW. Our point of departure is the regime of strong parent CDW, which may occur at the Van Hove singularity and ambient pressure. With a small density of states from the small Fermi pockets at \mathbf{M}'_α , the superconductivity holds a much weaker dimensionless coupling $V_s^a D$ than that of the parent CDW. This implies a large separation of energy scales between the two states. Therefore, the superconductivity develops at a much lower critical temperature. Since the system lies deeply in the parent CDW phase, the radial fluctuation is much weaker than the tangential fluctuations for the deformation energy. The leading Pomeranchuk fluctuations occur in the $d_{x^2-y^2,xy}$ -wave channels, which trigger the $(s + d_{x^2-y^2})$ - and d_{xy} -wave superconductivity in this regime.

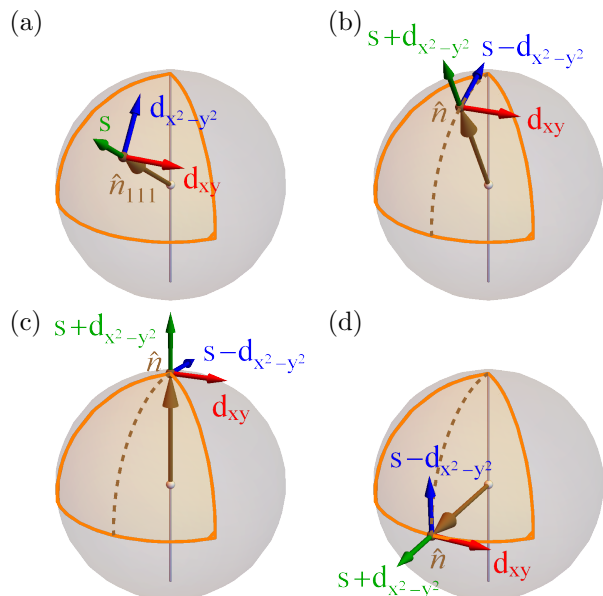


FIG. 4. Bloch sphere model of the deformation energy in the first octant (orange). (a) Under C_6 symmetry, the deformation energy sits at \hat{n}_{111} . The available fluctuations are indicated by the arrows. (b) Under the twofold symmetry along the $\alpha = 1$ direction (center vertical line), a shift occurs along the longitude (brown dashed curve). The deformation energy sits at the (c) north pole or (d) equatorial at the quantum critical point.

When a suppression occurs, the parent CDW exhibits a decreasing critical temperature. The Fermi pockets are enlarged accordingly, where the increasing density of states enhances the superconductivity and raises its critical temperature. Such an enhancement is significantly opposite to the trend of the parent CDW. If the first reconstructed Van Hove singularity occurs, the superconductivity arrives at a peak of the critical temperature [41, 55]. Further suppression of the parent CDW shifts the reconstructed Fermi surface away from the Van Hove singularity. With the density of states reduced, a suppression occurs to the superconducting critical temperature and marks the end of a superconducting dome. Due to the large diminishment of gap structures, the CDW may host strong fluctuations in all Pomeranchuk channels. This induces the strong fluctuations of superconductivity among all channels. A direct consequence is the broadened transition temperature window between T_c^{onset} and T_c^{zero} , where the resistivity starts to drop and vanishes, respectively. When the CDW is driven toward the quantum critical point, the superconductivity experiences a second enhancement from strong Pomeranchuk fluctuations and the second reconstructed Van Hove singularity. At the quantum critical point, the superconductivity becomes the leading instability in the unfolded theory. The leading channel in this second dome is intimately related to the driving interactions. If the pairing occurs from electronic repulsion, the superconductivity may develop in the leading $d_{x^2-y^2,xy}$ - or f -wave channels [53, 59, 65]. The former is consistent with the Pomeranchuk fluctuations and may be more preferable close to the quantum critical point. On the other hand, the superconductivity can also occur in the s -wave channel from phonon-mediated attraction. Whichever case occurs depends on the practical systems under study. Thus, our model predicts a ‘double dome’ structure of superconductivity under pressure, with the assumption that pressure suppresses the CDW either by shifting the Fermi level away from the Van Hove singularity, or by inducing a structural evolution [17, 46]. This is consistent with the experimental observations in the kagome metals AV_3Sb_5 [7, 22, 46]. Similar results have also been observed in uniaxial-strain measurements [26]. Notably, the reconstructed Van Hove singularity have been observed close to the Fermi level for $A = \text{Rb}$, despite different details in the band structures [20].

To understand the symmetry of the superconductivity in the kagome metals AV_3Sb_5 , we incorporate the experimentally observed C_6 symmetry breaking along the x axis. Such a symmetry breaking leads to the one-large-two-small or one-small-two-large structures of the Fermi pockets. The residual twofold symmetries include the C_2 inversion symmetry, as well as the (probably weaker) reflection symmetries with respect to the x and y axes. The irreducible pairing channels are indicated transparently by the Bloch sphere model of

the deformation energy. Under the symmetry breaking, a shift away from \hat{n}_{111} along the longitude [Fig. 4(b)] distinguishes the latitudinal and longitudinal channels. The latitudinal and according reflection-odd d_{xy} -wave channels remain invariant. Meanwhile, the radial and longitudinal channels are shifted together, which are related to the reflection-even ($s \pm d_{x^2-y^2}$)-wave channels. These channels host the patch representations $d_{\pm} = \cos\theta_{\pm}d_0 + \sin\theta_{\pm}d_1$ with $(\theta_+, \theta_-) = (\theta, \theta + \pi/2)$ at $\theta \in [\theta_{23}, \theta_1] = [\arctan(-1/\sqrt{2}), \arctan\sqrt{2}]$.

We first determine the leading channel in the first superconducting dome. Under a twofold symmetry, low-energy manifold generally spans along the latitude on the Bloch sphere. The latitudinal fluctuation is less costly, indicating the leading role of the d_{xy} -wave Pomeranchuk channel. The strong fluctuation then induces the d_{xy} -wave nematic spin-singlet superconductivity. Notably, this result is justified by the experimental observations. A measurement of thermal conductivity uncovers the nodal nature of the gap function [45], consistent with the nodes at $\alpha = 1$ in the patch representation d_2 . Meanwhile, the magnetoresistance under an in-plane magnetic field shows a one-strong-two-weak structure at the directions of \mathbf{M}'_{α} [49, 50]. Since magnetoresistance is negatively correlated to superconducting gap, the observed superconductivity exhibits a one-weak-two-strong gap function on the Fermi pockets. This observation is again consistent with the patch representation d_2 . Combining the theoretical and experimental analyses, we conclude that the first superconducting dome is occupied by the d_{xy} -wave nematic spin-singlet superconductivity.

Due to driving-interaction dependence and strong fluctuations, the leading channel in the second superconducting dome is less obvious from the theoretical model. At the quantum critical point, the deformation energy may develop at the north pole $\theta = \theta_1$ or equatorial $\theta = \theta_{23}$ [Figs. 4(c) or 4(d)]. The former carries a single strong component with leading radial fluctuation, while the latter hosts two strong components with leading radial and/or latitudinal fluctuations. For $A = \text{Rb}, \text{Cs}$ where the double-dome superconductivity is observed, the one-strong-two-weak CDW configurations suggest the specific answer in the first case [16, 19]. With the leading radial fluctuation, we infer the ($s + d_{x^2-y^2}$)-wave nematic spin-singlet superconductivity in the second superconducting dome. Future justification can be offered by, for example, the measurements of magnetoresistance under an in-plane magnetic field at high pressure [49, 50]. On the other hand, the result for $A = \text{K}$ is undetermined, as the one-strong-two-weak and one-weak-two-strong CDW configurations are both observed [5, 15]. The single-dome superconductivity [7] indicates that the first reconstructed Van Hove singularity is either absent or passed. Finally, the regime far above the quantum critical point is beyond our theoretical model.

In summary, we show that the reconstructed Pomer-

anchuk fluctuations in the parent CDW can drive the kagome superconductors. Our theoretical model offers a transparent interpretation to the experiments of kagome metals AV_3Sb_5 . The large difference of energy scales between the CDW and the superconductivity is interpreted from a ‘parent-child’ relationship. Moreover, the double-dome superconductivity is explained by the presence of two reconstructed Van Hove singularities. The symmetries of superconductivity are further determined in each dome. Our work sheds light on an unconventional pairing mechanism with strong evidences in the kagome metals AV_3Sb_5 . Note that the double-dome structure follows from the evolution of the density of states, and will be shared by any mechanism wherein the superconductivity arises from a weak-coupling instability of the reconstructed Fermi surface. It is also worth mentioning that the reconstructed bands may be topological [2, 3, 6, 43], where the superconductivity can receive geometric enhancement [66–70] or nontrivial topology. Spin-orbit coupling may also lead to additional features. Since Van Hove Fermi surface is universal on hexagonal lattices, our theoretical model also applies to the other hexagonal lattice systems. The systems with incommensurate CDW, such as graphene moiré systems [41], may also host strong reconstructed Pomeranchuk fluctuations from sliding phases. The study of according superconductivity serves as an interesting topic for future work.

Note added. While we were finalizing the manuscript, we learned about an independent study of superconductivity from CDW fluctuations in the kagome metals AV_3Sb_5 [71]. This work considered the pairing mechanism in the unfolded theory, which is eligible at the high critical pressure. Our analysis adopts the reconstructed band structures from the parent CDW, which captures more properly the situation at ambient pressure. It also explains the exotic double-dome superconductivity within the CDW phase at high pressure.

This research was sponsored by the Army Research Office and was accomplished under Grant No. W911NF-17-1-0482. The views and conclusions contained in this document are those of the authors and should not be interpreted as representing the official policies, either expressed or implied, of the Army Research Office or the U.S. Government. The U.S. Government is authorized to reproduce and distribute reprints for Government purposes notwithstanding any copyright notation herein. RN also acknowledges the support of the Alfred P. Sloan foundation through a Sloan Research Fellowship.

[1] B. R. Ortiz, L. C. Gomes, J. R. Morey, M. Winiarski, M. Bordelon, J. S. Mangum, I. W. H. Oswald, J. A. Rodriguez-Rivera, J. R. Neilson, S. D. Wilson, E. Ertekin, T. M. McQueen, and E. S. Toberer, “New kagome prototype materials: discovery of

kv_3sb_5 , rbv_3sb_5 , and csv_3sb_5 ,” *Phys. Rev. Materials* **3**, 094407 (2019).

[2] S.-Y. Yang, Y. Wang, B. R. Ortiz, D. Liu, J. Gayles, E. Derunova, R. Gonzalez-Hernandez, L. Šmejkal, Y. Chen, S. S. P. Parkin, S. D. Wilson, E. S. Toberer, T. McQueen, and M. N. Ali, “Giant, unconventional anomalous hall effect in the metallic frustrated magnet candidate, kv_3sb_5 ,” *Sci. Adv.* **6**, eabb6003 (2020).

[3] B. R. Ortiz, S. M. L. Teicher, Y. Hu, J. L. Zuo, P. M. Sarte, E. C. Schueller, A. M. M. Abeykoon, M. J. Krogstad, S. Rosenkranz, R. Osborn, R. Seshadri, L. Balents, J. He, and S. D. Wilson, “ Csv_3sb_5 : A z_2 topological kagome metal with a superconducting ground state,” *Phys. Rev. Lett.* **125**, 247002 (2020).

[4] E. M. Kenney, B. R. Ortiz, C. Wang, S. D. Wilson, and M. J. Graf, “Absence of local moments in the kagome metal KV_3sb_5 as determined by muon spin spectroscopy,” *J. Phys.: Condens. Matter* **33**, 235801 (2021).

[5] Y.-X. Jiang, J.-X. Yin, M. M. Denner, N. Shumiya, B. R. Ortiz, G. Xu, Z. Guguchia, J. He, M. Shafayat Hossain, X. Liu, J. Ruff, L. Kautzsch, S. S. Zhang, G. Chang, I. Belopolski, Q. Zhang, T. A. Cochran, D. Multer, M. Litskevich, Z.-J. Cheng, X. P. Yang, Z. Wang, R. Thomale, T. Neupert, S. D. Wilson, and M. Zahid Hasan, “Discovery of unconventional chiral charge order in kagome superconductor KV_3Sb_5 ,” arXiv e-prints , arXiv:2012.15709 (2020), [arXiv:2012.15709 \[cond-mat.supr-con\]](https://arxiv.org/abs/2012.15709).

[6] F. H. Yu, T. Wu, Z. Y. Wang, B. Lei, W. Z. Zhuo, J. J. Ying, and X. H. Chen, “Concurrence of anomalous hall effect and charge density wave in a superconducting topological kagome metal,” *Phys. Rev. B* **104**, L041103 (2021).

[7] F. Du, S. Luo, B. R. Ortiz, Y. Chen, W. Duan, D. Zhang, X. Lu, S. D. Wilson, Y. Song, and H. Yuan, “Pressure-induced double superconducting domes and charge instability in the kagome metal kv_3sb_5 ,” *Phys. Rev. B* **103**, L220504 (2021).

[8] H. Zhao, H. Li, B. R. Ortiz, S. M. L. Teicher, T. Park, M. Ye, Z. Wang, L. Balents, S. D. Wilson, and I. Zeljkovic, “Cascade of correlated electron states in a kagome superconductor CsV_3Sb_5 ,” arXiv e-prints , arXiv:2103.03118 (2021), [arXiv:2103.03118 \[cond-mat.supr-con\]](https://arxiv.org/abs/2103.03118).

[9] Z. Liang, X. Hou, W. Ma, F. Zhang, P. Wu, Z. Zhang, F. Yu, J. J. Ying, K. Jiang, L. Shan, Z. Wang, and X. H. Chen, “Three-dimensional charge density wave and robust zero-bias conductance peak inside the superconducting vortex core of a kagome superconductor CsV_3Sb_5 ,” arXiv e-prints , arXiv:2103.04760 (2021), [arXiv:2103.04760 \[cond-mat.supr-con\]](https://arxiv.org/abs/2103.04760).

[10] E. Uykur, B. R. Ortiz, S. D. Wilson, M. Dressel, and A. A. Tsirlin, “Optical detection of charge-density-wave instability in the non-magnetic kagome metal KV_3Sb_5 ,” arXiv e-prints , arXiv:2103.07912 (2021), [arXiv:2103.07912 \[cond-mat.str-el\]](https://arxiv.org/abs/2103.07912).

[11] H. Chen, H. Yang, B. Hu, Z. Zhao, J. Yuan, Y. Xing, G. Qian, Z. Huang, G. Li, Y. Ye, Q. Yin, C. Gong, Z. Tu, H. Lei, S. Ma, H. Zhang, S. Ni, H. Tan, C. Shen, X. Dong, B. Yan, Z. Wang, and H.-J. Gao, “Roton pair density wave and unconventional strong-coupling superconductivity in a topological kagome metal,” arXiv e-prints , arXiv:2103.09188 (2021), [arXiv:2103.09188 \[cond-mat.supr-con\]](https://arxiv.org/abs/2103.09188).

- [12] H. X. Li, T. T. Zhang, Y. Y. Pai, C. Marvinney, A. Said, T. Yilmaz, Q. Yin, C. Gong, Z. Tu, E. Vescovo, R. G. Moore, S. Murakami, H. C. Lei, H. N. Lee, B. Lawrie, and H. Miao, “Observation of Unconventional Charge Density Wave without Acoustic Phonon Anomaly in Kagome Superconductors AV_3Sb_5 ($A=Rb,Cs$),” arXiv e-prints , arXiv:2103.09769 (2021), [arXiv:2103.09769 \[cond-mat.supr-con\]](#).
- [13] Z. Wang, S. Ma, Y. Zhang, H. Yang, Z. Zhao, Y. Ou, Y. Zhu, S. Ni, Z. Lu, H. Chen, K. Jiang, L. Yu, Y. Zhang, X. Dong, J. Hu, H.-J. Gao, and Z. Zhao, “Distinctive momentum dependent charge-density-wave gap observed in CsV_3Sb_5 superconductor with topological Kagome lattice,” arXiv e-prints , arXiv:2104.05556 (2021), [arXiv:2104.05556 \[cond-mat.supr-con\]](#).
- [14] K. Nakayama, Y. Li, M. Liu, Z. Wang, T. Takahashi, Y. Yao, and T. Sato, “Multiple Energy Scales and Anisotropic Energy Gap in the Charge-Density-Wave Phase of Kagome Superconductor CsV_3Sb_5 ,” arXiv e-prints , arXiv:2104.08042 (2021), [arXiv:2104.08042 \[cond-mat.supr-con\]](#).
- [15] H. Li, H. Zhao, B. R. Ortiz, T. Park, M. Ye, L. Balents, Z. Wang, S. D. Wilson, and I. Zeljkovic, “Rotation symmetry breaking in the normal state of a kagome superconductor KV_3Sb_5 ,” arXiv e-prints , arXiv:2104.08209 (2021), [arXiv:2104.08209 \[cond-mat.supr-con\]](#).
- [16] N. Shumiya, M. Shafayat Hossain, J.-X. Yin, Y.-X. Jiang, B. R. Ortiz, H. Liu, Y. Shi, Q. Yin, H. Lei, S. S. Zhang, G. Chang, Q. Zhang, T. A. Cochran, D. Multer, M. Litskevich, Z.-J. Cheng, X. P. Yang, Z. Guguchia, S. D. Wilson, and M. Zahid Hasan, “Tunable chiral charge order in kagome superconductor RbV_3Sb_5 ,” arXiv e-prints , arXiv:2105.00550 (2021), [arXiv:2105.00550 \[cond-mat.str-el\]](#).
- [17] A. A. Tsirlin, P. Fertey, B. R. Ortiz, B. Klis, V. Merkl, M. Dressel, S. D. Wilson, and E. Uykur, “Anisotropic compression and role of Sb in the superconducting kagome metal CsV_3Sb_5 ,” arXiv e-prints , arXiv:2105.01397 (2021), [arXiv:2105.01397 \[cond-mat.supr-con\]](#).
- [18] M. Kang, S. Fang, J.-K. Kim, B. R. Ortiz, J. Yoo, B.-G. Park, S. D. Wilson, J.-H. Park, and R. Comin, “Twofold van Hove singularity and origin of charge order in topological kagome superconductor CsV_3Sb_5 ,” arXiv e-prints , arXiv:2105.01689 (2021), [arXiv:2105.01689 \[cond-mat.str-el\]](#).
- [19] Z. Wang, Y.-X. Jiang, Y. Li, J.-X. Yin, G.-Y. Wang, H.-L. Huang, J. Liu, P. Zhu, N. Shumiya, M. Shafayat Hossain, H. Liu, Y. Shi, J. Duan, X. Li, G. Chang, P. Dai, H. Zheng, J. Jia, M. Zahid Hasan, and Y. Yao, “Anomalous transport and chiral charge order in kagome superconductor CsV_3Sb_5 ,” arXiv e-prints , arXiv:2105.04542 (2021), [arXiv:2105.04542 \[cond-mat.str-el\]](#).
- [20] S. Cho, H. Ma, W. Xia, Y. Yang, Z. Liu, Z. Huang, Z. Jiang, X. Lu, J. Liu, Z. Liu, J. Jia, Y. Guo, J. Liu, and D. Shen, “Emergence of new van Hove singularities in the charge density wave state of a topological kagome metal RbV_3Sb_5 ,” arXiv e-prints , arXiv:2105.05117 (2021), [arXiv:2105.05117 \[cond-mat.supr-con\]](#).
- [21] B. Q. Song, X. M. Kong, W. Xia, Q. W. Yin, C. P. Tu, C. C. Zhao, D. Z. Dai, K. Meng, Z. C. Tao, Z. J. Tu, C. S. Gong, H. C. Lei, Y. F. Guo, X. F. Yang, and S. Y. Li, “Competing superconductivity and charge-density wave in Kagome metal CsV_3Sb_5 : evidence from their evolutions with sample thickness,” arXiv e-prints , arXiv:2105.09248 (2021), [arXiv:2105.09248 \[cond-mat.supr-con\]](#).
- [22] F. H. Yu, D. H. Ma, W. Z. Zhuo, S. Q. Liu, X. K. Wen, B. Lei, J. J. Ying, and X. H. Chen, “Unusual competition of superconductivity and charge-density-wave state in a compressed topological kagome metal,” *Nat. Commun.* **12**, 3645 (2021).
- [23] Y. Hu, X. Wu, B. R. Ortiz, S. Ju, X. Han, J. Z. Ma, N. C. Plumb, M. Radovic, R. Thomale, S. D. Wilson, A. P. Schnyder, and M. Shi, “Rich Nature of Van Hove Singularities in Kagome Superconductor CsV_3Sb_5 ,” arXiv e-prints , arXiv:2106.05922 (2021), [arXiv:2106.05922 \[cond-mat.supr-con\]](#).
- [24] I. Mielke, C., D. Das, J. X. Yin, H. Liu, R. Gupta, C. N. Wang, Y. X. Jiang, M. Medarde, X. Wu, H. C. Lei, J. J. Chang, P. Dai, Q. Si, H. Miao, R. Thomale, T. Neupert, Y. Shi, R. Khasanov, M. Z. Hasan, H. Luetkens, and Z. Guguchia, “Time-reversal symmetry-breaking charge order in a correlated kagome superconductor,” arXiv e-prints , arXiv:2106.13443 (2021), [arXiv:2106.13443 \[cond-mat.mtrl-sci\]](#).
- [25] H. Luo, Q. Gao, H. Liu, Y. Gu, D. Wu, C. Yi, J. Jia, S. Wu, X. Luo, Y. Xu, L. Zhao, Q. Wang, H. Mao, G. Liu, Z. Zhu, Y. Shi, K. Jiang, J. Hu, Z. Xu, and X. J. Zhou, “Electronic Nature of Charge Density Wave and Electron-Phonon Coupling in Kagome Superconductor KV_3Sb_5 ,” arXiv e-prints , arXiv:2107.02688 (2021), [arXiv:2107.02688 \[cond-mat.supr-con\]](#).
- [26] T. Qian, M. H. Christensen, C. Hu, A. Saha, B. M. Andersen, R. M. Fernandes, T. Birol, and N. Ni, “Revealing the competition between charge-density wave and superconductivity in CsV_3Sb_5 through uniaxial strain,” arXiv e-prints , arXiv:2107.04545 (2021), [arXiv:2107.04545 \[cond-mat.supr-con\]](#).
- [27] H. Tan, Y. Liu, Z. Wang, and B. Yan, “Charge density waves and electronic properties of superconducting kagome metals,” arXiv e-prints , arXiv:2103.06325 (2021), [arXiv:2103.06325 \[cond-mat.supr-con\]](#).
- [28] X. Feng, K. Jiang, Z. Wang, and J. Hu, “Chiral flux phase in the Kagome superconductor AV_3Sb_5 ,” arXiv e-prints , arXiv:2103.07097 (2021), [arXiv:2103.07097 \[cond-mat.supr-con\]](#).
- [29] M. M. Denner, R. Thomale, and T. Neupert, “Analysis of charge order in the kagome metal AV_3Sb_5 ($A =K,Rb,Cs$),” arXiv e-prints , arXiv:2103.14045 (2021), [arXiv:2103.14045 \[cond-mat.str-el\]](#).
- [30] Y.-P. Lin and R. M. Nandkishore, “Complex charge density waves at van hove singularity on hexagonal lattices: Haldane-model phase diagram and potential realization in the kagome metals aV_3sb_5 ($a=k, rb, cs$),” *Phys. Rev. B* **104**, 045122 (2021).
- [31] T. Park, M. Ye, and L. Balents, “Electronic instabilities of kagome metals: saddle points and Landau theory,” arXiv e-prints , arXiv:2104.08425 (2021), [arXiv:2104.08425 \[cond-mat.str-el\]](#).
- [32] C. Setty, H. Hu, L. Chen, and Q. Si, “Electron correlations and T -breaking density wave order in a Z_2 kagome metal,” arXiv e-prints , arXiv:2105.15204 (2021), [arXiv:2105.15204 \[cond-mat.str-el\]](#).
- [33] X. Feng, Y. Zhang, K. Jiang, and J. Hu, “Low-energy effective theory and symmetry classification of flux phases on Kagome lattice,” arXiv e-prints , arXiv:2106.04395 (2021), [arXiv:2106.04395 \[cond-mat.str-el\]](#).

- [34] H. Miao, H. X. Li, H. N. Lee, A. Said, H. C. Lei, J. X. Yin, M. Z. Hasan, Z. Wang, H. Tan, and B. Yan, “Geometry of the charge density wave in kagome metal AV_3Sb_5 ,” arXiv e-prints, arXiv:2106.10150 (2021), [arXiv:2106.10150 \[cond-mat.str-el\]](#).
- [35] M. H. Christensen, T. Birol, B. M. Andersen, and R. M. Fernandes, “Theory of the charge-density wave in AV_3Sb_5 kagome metals,” arXiv e-prints, arXiv:2107.04546 (2021), [arXiv:2107.04546 \[cond-mat.supr-con\]](#).
- [36] I. Affleck and J. B. Marston, “Large- n limit of the heisenberg-hubbard model: Implications for high- T_c superconductors,” *Phys. Rev. B* **37**, 3774 (1988).
- [37] C. M. Varma, “Non-fermi-liquid states and pairing instability of a general model of copper oxide metals,” *Phys. Rev. B* **55**, 14554 (1997).
- [38] C. Nayak, “Density-wave states of nonzero angular momentum,” *Phys. Rev. B* **62**, 4880 (2000).
- [39] S. Chakravarty, R. B. Laughlin, D. K. Morr, and C. Nayak, “Hidden order in the cuprates,” *Phys. Rev. B* **63**, 094503 (2001).
- [40] J. W. F. Venderbos, “Symmetry analysis of translational symmetry broken density waves: Application to hexagonal lattices in two dimensions,” *Phys. Rev. B* **93**, 115107 (2016).
- [41] Y.-P. Lin and R. M. Nandkishore, “Chiral twist on the high- T_c phase diagram in moiré heterostructures,” *Phys. Rev. B* **100**, 085136 (2019).
- [42] Y.-P. Lin, “Higher-order topological insulators from $3Q$ charge bond orders on hexagonal lattices: A hint to kagome metals,” arXiv e-prints, arXiv:2106.09717 (2021), [arXiv:2106.09717 \[cond-mat.str-el\]](#).
- [43] B. R. Ortiz, P. M. Sarte, E. M. Kenney, M. J. Graf, S. M. L. Teicher, R. Seshadri, and S. D. Wilson, “Superconductivity in the z_2 kagome metal kV_3Sb_5 ,” *Phys. Rev. Materials* **5**, 034801 (2021).
- [44] Y. Wang, S. Yang, P. K. Sivakumar, B. R. Ortiz, S. M. L. Teicher, H. Wu, A. K. Srivastava, C. Garg, D. Liu, S. S. P. Parkin, E. S. Toberer, T. McQueen, S. D. Wilson, and M. N. Ali, “Proximity-induced spin-triplet superconductivity and edge supercurrent in the topological Kagome metal, $K_{1-x}V_3Sb_5$,” arXiv e-prints, arXiv:2012.05898 (2020), [arXiv:2012.05898 \[cond-mat.supr-con\]](#).
- [45] C. C. Zhao, L. S. Wang, W. Xia, Q. W. Yin, J. M. Ni, Y. Y. Huang, C. P. Tu, Z. C. Tao, Z. J. Tu, C. S. Gong, H. C. Lei, Y. F. Guo, X. F. Yang, and S. Y. Li, “Nodal superconductivity and superconducting domes in the topological Kagome metal CsV_3Sb_5 ,” arXiv e-prints, arXiv:2102.08356 (2021), [arXiv:2102.08356 \[cond-mat.supr-con\]](#).
- [46] K. Y. Chen, N. N. Wang, Q. W. Yin, Y. H. Gu, K. Jiang, Z. J. Tu, C. S. Gong, Y. Uwatoko, J. P. Sun, H. C. Lei, J. P. Hu, and J.-G. Cheng, “Double superconducting dome and triple enhancement of T_c in the kagome superconductor csv_3sb_5 under high pressure,” *Phys. Rev. Lett.* **126**, 247001 (2021).
- [47] W. Duan, Z. Nie, S. Luo, F. Yu, B. R. Ortiz, L. Yin, H. Su, F. Du, A. Wang, Y. Chen, X. Lu, J. Ying, S. D. Wilson, X. Chen, Y. Song, and H. Yuan, “Nodeless superconductivity in the kagome metal CsV_3Sb_5 ,” arXiv e-prints, arXiv:2103.11796 (2021), [arXiv:2103.11796 \[cond-mat.supr-con\]](#).
- [48] Z. Zhang, Z. Chen, Y. Zhou, Y. Yuan, S. Wang, J. Wang, H. Yang, C. An, L. Zhang, X. Zhu, Y. Zhou, X. Chen, J. Zhou, and Z. Yang, “Pressure-induced reemergence of superconductivity in the topological kagome metal Csv_3sb_5 ,” *Phys. Rev. B* **103**, 224513 (2021).
- [49] S. Ni, S. Ma, Y. Zhang, J. Yuan, H. Yang, Z. Lu, N. Wang, J. Sun, Z. Zhao, D. Li, S. Liu, H. Zhang, H. Chen, K. Jin, J. Cheng, L. Yu, F. Zhou, X. Dong, J. Hu, H.-J. Gao, and Z. Zhao, “Anisotropic superconducting properties of kagome metal CsV_3sb_5 ,” *Chin. Phys. Lett.* **38**, 057403 (2021).
- [50] Y. Xiang, Q. Li, Y. Li, W. Xie, H. Yang, Z. Wang, Y. Yao, and H.-H. Wen, “Twofold symmetry of c -axis resistivity in topological kagome superconductor CsV_3Sb_5 with in-plane rotating magnetic field,” arXiv e-prints, arXiv:2104.06909 (2021), [arXiv:2104.06909 \[cond-mat.supr-con\]](#).
- [51] H.-S. Xu, Y.-J. Yan, R. Yin, W. Xia, S. Fang, Z. Chen, Y. Li, W. Yang, Y. Guo, and D.-L. Feng, “Multiband superconductivity with sign-preserving order parameter in kagome superconductor CsV_3Sb_5 ,” arXiv e-prints, arXiv:2104.08810 (2021), [arXiv:2104.08810 \[cond-mat.supr-con\]](#).
- [52] C. C. Zhu, X. F. Yang, W. Xia, Q. W. Yin, L. S. Wang, C. C. Zhao, D. Z. Dai, C. P. Tu, B. Q. Song, Z. C. Tao, Z. J. Tu, C. S. Gong, H. C. Lei, Y. F. Guo, and S. Y. Li, “Double-dome superconductivity under pressure in the V-based Kagome metals AV_3Sb_5 ($A = Rb$ and K),” arXiv e-prints, arXiv:2104.14487 (2021), [arXiv:2104.14487 \[cond-mat.supr-con\]](#).
- [53] X. Wu, T. Schwemmer, T. Müller, A. Consiglio, G. Sangiovanni, D. Di Sante, Y. Iqbal, W. Hanke, A. P. Schnyder, M. M. Denner, M. H. Fischer, T. Neupert, and R. Thomale, “Nature of unconventional pairing in the kagome superconductors AV_3Sb_5 ,” arXiv e-prints, arXiv:2104.05671 (2021), [arXiv:2104.05671 \[cond-mat.supr-con\]](#).
- [54] L. Van Hove, “The occurrence of singularities in the elastic frequency distribution of a crystal,” *Phys. Rev.* **89**, 1189 (1953).
- [55] R. Nandkishore, L. S. Levitov, and A. V. Chubukov, “Chiral superconductivity from repulsive interactions in doped graphene,” *Nat. Phys.* **8**, 158 (2012).
- [56] M. L. Kiesel, C. Platt, W. Hanke, D. A. Abanin, and R. Thomale, “Competing many-body instabilities and unconventional superconductivity in graphene,” *Phys. Rev. B* **86**, 020507 (2012).
- [57] M. L. Kiesel, C. Platt, and R. Thomale, “Unconventional fermi surface instabilities in the kagome hubbard model,” *Phys. Rev. Lett.* **110**, 126405 (2013).
- [58] W.-S. Wang, Z.-Z. Li, Y.-Y. Xiang, and Q.-H. Wang, “Competing electronic orders on kagome lattices at van hove filling,” *Phys. Rev. B* **87**, 115135 (2013).
- [59] R. Nandkishore, R. Thomale, and A. V. Chubukov, “Superconductivity from weak repulsion in hexagonal lattice systems,” *Phys. Rev. B* **89**, 144501 (2014).
- [60] L. Classen, A. V. Chubukov, C. Honerkamp, and M. M. Scherer, “Competing orders at higher-order van hove points,” *Phys. Rev. B* **102**, 125141 (2020).
- [61] Y.-P. Lin and R. M. Nandkishore, “Parquet renormalization group analysis of weak-coupling instabilities with multiple high-order van hove points inside the brillouin zone,” *Phys. Rev. B* **102**, 245122 (2020).
- [62] R. M. Fernandes and A. J. Millis, “Nematicity as a probe of superconducting pairing in iron-based superconductors,” *Phys. Rev. Lett.* **111**, 127001 (2013).

- [63] R. M. Fernandes, A. V. Chubukov, and J. Schmalian, “What drives nematic order in iron-based superconductors?” *Nat. Phys.* **10**, 97 (2014).
- [64] X. Chen, S. Maiti, R. M. Fernandes, and P. J. Hirschfeld, “Nematicity and superconductivity: Competition versus cooperation,” *Phys. Rev. B* **102**, 184512 (2020).
- [65] Y.-P. Lin and R. M. Nandkishore, “Kohn-luttinger superconductivity on two orbital honeycomb lattice,” *Phys. Rev. B* **98**, 214521 (2018).
- [66] S. Peotta and P. Törmä, “Superfluidity in topologically nontrivial flat bands,” *Nat. Commun.* **6**, 8944 (2015).
- [67] L. Liang, T. I. Vanhala, S. Peotta, T. Siro, A. Harju, and P. Törmä, “Band geometry, berry curvature, and superfluid weight,” *Phys. Rev. B* **95**, 024515 (2017).
- [68] X. Hu, T. Hyart, D. I. Pikulin, and E. Rossi, “Geometric and conventional contribution to the superfluid weight in twisted bilayer graphene,” *Phys. Rev. Lett.* **123**, 237002 (2019).
- [69] F. Xie, Z. Song, B. Lian, and B. A. Bernevig, “Topology-bounded superfluid weight in twisted bilayer graphene,” *Phys. Rev. Lett.* **124**, 167002 (2020).
- [70] Y.-P. Lin and W.-H. Hsiao, “Dual haldane sphere and quantized band geometry in chiral multifold fermions,” *Phys. Rev. B* **103**, L081103 (2021).
- [71] R. Tazai, Y. Yamakawa, S. Onari, and H. Kontani, “Mechanism of exotic density-wave and beyond-Migdal unconventional superconductivity in kagome metal AV₃Sb₅ (A=K, Rb, Cs),” arXiv e-prints, arXiv:2107.05372 (2021), arXiv:2107.05372 [cond-mat.supr-con].